

ARTICLE

Open Access

Highly sensitive and flexible pressure sensors using position- and dimension-controlled ZnO nanotube arrays grown on graphene films

Jun Beom Park¹, Minh S. Song¹, Ramesh Ghosh¹, Rajendra Kumar Saroj¹, Yunjae Hwang¹, Youngbin Tchoe², Hongseok Oh², Hyeonjun Baek³, Yoonseo Lim⁴, Bosung Kim⁵, Sang-Woo Kim⁵ and Gyu-Chul Yi^{1,6}

Abstract

A facile and novel technique for the fabrication of pressure sensors is reported based on the hybridization of one-dimensional nanomaterials and two-dimensional graphene film. In particular, piezoelectric pressure sensors are fabricated by using vertically aligned and position- and dimension-controlled ZnO nanotube arrays grown on graphene layers. Graphene layers act not only as substrates for catalyst-free growth of high-quality ZnO nanotubes but also as flexible conduction channels connecting ZnO nanotubes and metal electrodes. Freestanding and flexible sensors have been efficiently obtained via mechanical lift-off of hybrid ZnO nanotube/graphene film structures and by exploiting the weak van der Waals forces existing between the graphene film and the original substrates. A prototype of such devices shows a high pressure sensitivity (-4.4 kPa^{-1}), which would enable the detection of weak flows of inert gas. The relatively low wall thickness and large length of the ZnO nanotubes suggest a relatively high sensitivity to external pressures. The obtained nanotube sensors are attached to the philtrum and wrist of a volunteer and used to monitor his breath and heart rate. Overall, the prototype hybrid sensing device has great potential as wearable technology, especially in the sector of advanced healthcare devices.

Introduction

One-dimensional (1D) piezoelectric nanomaterials have attracted tremendous attention due to their diverse applications, including with sensors and self-powered devices^{1–12}. In particular, the tiny contact areas between 1D inorganic nanomaterials and their flexible supporting substrates have enabled the fabrication of mechanically flexible devices^{13,14}. Conventionally, flexible piezoelectric pressure sensors have been fabricated using composite polymers with conductive fillers (e.g., carbon nanotubes, metallic nanofibers, and nanoparticles)^{15–17}. However, the sensing performance of

pressure sensors based on low-cost composite elastomers with planar structures can degrade in the ambient atmosphere. Moreover, flexible piezoelectric devices based on 1D inorganic nanomaterials have superior properties since they exploit the high sensitivity and reliability of such materials. Among the known piezoelectric material systems, ZnO-based nanotubes/nanowires have been considered highly advantageous for piezoelectric devices due to their high responsivity^{2–5,17,18}. Despite the superior performances demonstrated by 1D inorganic nanomaterials, the manufacturing of pressure-sensing devices based on inorganic materials has encountered some obstacles. First, the controlled growth of high-quality 1D inorganic nanomaterials requires single-crystal substrates¹⁹. This has hindered the fabrication of low-cost 1D nanostructures with large areas. Second, the combination of 1D nanomaterials with flexible substrates is difficult due to the lack of reliable and high-yield processes for lift-off of 1D nanomaterials. These

Correspondence: Ramesh Ghosh (Ramesh.Ghosh@glasgow.ac.uk) or Gyu-Chul Yi (gcyi@snu.ac.kr)

¹Department of Physics and Astronomy and Institute of Applied Physics, Seoul National University, Seoul 08826, South Korea

²Department of Electrical and Computer Engineering, University of California San Diego, La Jolla, CA 92093, USA

Full list of author information is available at the end of the article
These authors contributed equally: Jun Beom Park, Minh S. Song

© The Author(s) 2021



Open Access This article is licensed under a Creative Commons Attribution 4.0 International License, which permits use, sharing, adaptation, distribution and reproduction in any medium or format, as long as you give appropriate credit to the original author(s) and the source, provide a link to the Creative Commons license, and indicate if changes were made. The images or other third party material in this article are included in the article's Creative Commons license, unless indicated otherwise in a credit line to the material. If material is not included in the article's Creative Commons license and your intended use is not permitted by statutory regulation or exceeds the permitted use, you will need to obtain permission directly from the copyright holder. To view a copy of this license, visit <http://creativecommons.org/licenses/by/4.0/>.

difficulties can be circumvented by using graphene film as a growth template^{13,20}. It has been demonstrated that high-quality ZnO nanostructures can be grown on graphene film without using any catalyst²¹. Since the catalyst-free growth method tends to decrease the incorporation of impurities, it allows the growth of high-quality material^{22–24}. Furthermore, the ZnO nanostructures on the graphene film can be lifted off readily from the original substrates due to the existence of weak van der Waals forces between the graphene film and the substrates. Hence, hybrid structures of ZnO nanotubes/graphene can be considered promising for addressing the challenges associated with the fabrication of flexible and wearable pressure sensors.

Here we demonstrate the fabrication of flexible and high-sensitivity 1D piezoelectric pressure sensors containing ZnO nanotube arrays grown on chemical vapor deposition (CVD) graphene film, as well as their application to wearable health monitoring devices.

Materials and methods

Preparation of CVD graphene

A large-area, multilayered graphene film was synthesized on a Cu foil using a typical CVD method. First, the Cu foil surface was cleaned using acetone and isopropanol, and the foil was inserted into a tubular quartz chamber. The chamber was heated to 1030 °C with a continuous H₂ flow at 100 standard cubic centimeters per min (sccm) and 200 Torr. After the Cu foil reached 1030 °C, it was annealed for 15 min to coarsen its grains while maintaining a constant flow rate and reactor pressure. Then the graphene film was grown on the Cu foil for 130 min under a mixture of CH₄ and H₂ at flow rates of 10 and 100 sccm, respectively. During the growth process, the reactor pressure was maintained at 220 Torr. Finally, the sample was cooled to room temperature under a H₂ atmosphere while maintaining the chamber pressure of 200 Torr.

Preparation of substrates for the growth of ZnO nanotubes

Graphene was transferred onto a SiO₂-coated Si (SiO₂/Si) substrate. After that, a thin (50-nm) SiO₂ layer was deposited onto the as-transferred CVD graphene layer using a commercial plasma-enhanced CVD system. The oxide layer was annealed at 600 °C in O₂ to reduce the number of defects in the as-deposited SiO₂ structure and avoid undesired growth and reduce growth selectivity. Next, hole patterns were defined on the growth mask by electron-beam lithography. The SiO₂ film was dry-etched using CF₄ plasma and then wet-etched using a buffered oxide etchant (BOE). The residual oxide layer left on the graphene layer after dry etching was completely removed using BOE. After that, the substrate was cleaned in acetone, 2-propanol, and nitric acid and finally rinsed in deionized water to obtain selectively exposed array patterns on the graphene.

Growth of ZnO nanotubes on the CVD graphene film

Position-controlled ZnO nanotube arrays were grown on the CVD graphene film using metal organic CVD (MOCVD) with a homemade system. The growth of ZnO nanotubes has been described in detail previously. ZnO nanotubes were grown on the selectively exposed graphene layer mentioned in the previous section by using catalyst-free MOCVD. High-purity diethylzinc (DEZn) (>99.9999%) and high-purity O₂ (>99.995%) were used as reactants, while high-purity Ar (>99.999%) was used as the carrier gas. The flow rates of DEZn and O₂ were 40 and 100 sccm, respectively. During the growth process, Ar flowed into the quartz reactor with DEZn through a bubbler kept at a temperature of −10 °C. To prevent a premature reaction, the O₂ gas line was separated from the main gas manifold line. The reactor pressure was kept at 3.2 Torr, while the temperature remained at 690 °C during the growth process. Dimension- and position-controlled ZnO nanotube arrays were obtained on the e-beam lithography-patterned and selectively exposed graphene layers.

Lateral growth of the ZnO nanotubes

Lateral growth of the ZnO nanotubes was performed in another MOCVD chamber to tune the tube wall thickness. The gases and precursor used in this case were the same as those used for the first growth of the ZnO nanotubes, but the conditions were different: the flow rates of DEZn and O₂ were 2 and 8 sccm, respectively, the reactor pressure was kept at 8 Torr, and the temperature was maintained at 470 °C during the entire process.

Fabrication of the pressure sensors

To fabricate the top and bottom electrodes, an efficient lift-off process was applied. First, after preparing the ZnO nanotube arrays on the CVD graphene layers, a polyimide (PI) layer (VTEC™ PI) was created on the sample by spin coating at 2000 rpm. After that, the PI layer was prebaked at 120 °C for 120 s to completely evaporate the solvents. The PI layer mostly formed on the bottom side of the ZnO nanotubes, creating a thin coating on their tips. The PI layer on these tips was then selectively etched via an O plasma treatment (Plasma Prep II) for 5 min at 50 mA and 50 mTorr. Afterward, the entire layer was mechanically lifted from the substrate with the aid of a Kapton tape frame: the graphene film was separated from the loosely bonded SiO₂ substrate. The freestanding PI layer composed of ZnO nanotube/graphene layers was cured in a N₂ atmosphere within a homemade rapid thermal annealing system by two-step curing (at 200 °C for 3 min and at 300 °C for 3 min).

After completion of the lift-off process, a 100-nm Au layer was deposited on the exposed tips of the ZnO nanotubes, creating Schottky junctions. Subsequently, the freestanding nanotube arrays were flipped, and a 10/90-nm Cr/Au layer was deposited on the bottom side to

create ohmic contacts between ZnO, graphene, Cr, and Au. The freestanding pressure sensor devices were finally transferred to foreign rigid substrates to define their pressure response characteristics.

Morphological and structural characterization

Morphologies of the ZnO nanotube arrays and the fabricated pressure sensor devices were investigated using a field emission scanning electron microscope (FESEM; TESCAN) operated at 30 kV. This same system was also used to realize e-beam lithography of the metal hole array and examine its morphology.

Measurement of pressure responses when pressure was applied through a voice coil motor (VCM)

Mechanical force was applied to the sensor devices via a sapphire stamp attached to the axis of a VCM tool, which is capable of generating a certain force when placed in a magnetic field and subjected to electric current. The force controller measured the applied force with a precision of 0.001 N. A constant pressure was achieved by interfacing software (between the force controller and the Personal Computer (PC)). Each device was firmly attached on a flat surface so that one surface could be subjected to a vertical force. Notably, a smooth sapphire substrate ($3 \times 3 \text{ mm}^2$) was placed between the VCM force applying tip and the sensor to avoid the formation of unnecessary electrical pathways. The amount of pressure applied was calculated based on the force exerted by the $3 \times 3 \text{ mm}^2$ sapphire stamp on each device. A bias voltage of 0.4–2 V was applied to each device via a Keithley-2601 Sourcemeter; moreover, the freestanding pressure sensor devices were covered by a protective polymer (poly(methyl methacrylate) (PMMA)) layer to avoid mechanical damage.

The pressure responses of the devices were estimated from the current variation ratio ($\Delta I/I_0 = (I - I_0)/I_0$, where I and I_0 are the currents that occurred in the presence and absence of pressure, respectively). Furthermore, the sensitivity (S) was calculated from the following linear equation $S = \Delta(\Delta I/I_0)/\Delta p$.

Measurement of pressure responses when pressure was applied through a mass flow controller (MFC)

A constant flow of inert gas was applied and monitored by using an MFC, which imparted a uniform and constant pressure to the sensor. Each pressure sensor was placed on a solid substance 2 mm from the outlet of the MFC. To estimate the pressure of the constant gas flow, an electronic balance was placed 2 mm below the MFC. The constant mass flow of gas molecules was found to influence the electronic balance measurements. Considering the short-range streaming line of the gas flow (in the absence of external turbulences), we

decided to calculate the pressure exerted by the gas flow by dividing the weight obtained from the flux diameter. The pressure exerted by the gas flow at a constant rate was then calibrated by using an electronic balance with an accuracy of 0.1 mg. Since there was no direct contact between the force applying tool and the sensor, no protective PMMA layer was required.

Measurement of the breath and pulse responses

Breath- and pulse-sensing experiments were performed by attaching the sensor externally to the philtrum and wrist of a target person. The target persons were selected from among the co-authors from Seoul National University with full concern for ethical issues.

Results and discussion

Highly sensitive and flexible ZnO nanotube pressure sensors were successfully fabricated using position- and dimension-controlled ZnO nanotube arrays grown on CVD graphene films²⁰. Figure 1a contains a schematic illustration of the process used to fabricate the ZnO nanotube pressure sensors on CVD graphene film. First, ZnO nanotubes with outer diameters of 200–300 nm and heights of 15–18 μm were selectively grown on a patterned SiO_2/CVD graphene film²⁰. A FESEM image of the as-grown ZnO nanotube arrays is shown in Fig. 1b. It should be noted that the ZnO nanotubes were slightly tapered toward the top ends, resulting in a reduced end diameter. Figure S1 indicates that the effective diameters at the top ends of the nanotubes were 340 ± 20 and 814 ± 25 nm, corresponding to nanotubes with patterned (base) diameters of 500 nm and 1 μm , respectively. However, PI was coated on the ZnO nanotube arrays as an insulating layer and partially etched using an O plasma asher to expose the tips of the ZnO nanotube arrays. To fabricate flexible devices, the PI-coated nanotube arrays were mechanically lifted from the original substrates. Due to the presence of only a weak van der Waals force operating between the graphene film and the underneath SiO_2 substrate, the nanotube array could be easily lifted. After this passage, a 100-nm Au layer was deposited on the exposed tips of the ZnO nanotubes to form Schottky junctions. Subsequently, the freestanding nanotube arrays were flipped, and a Cr/Au film (10/90 nm) was deposited on their bottom side to create an ohmic contact between ZnO, graphene, Cr, and Au. A cross-sectional schematic diagram of one entire device is illustrated in the last panel of Fig. 1a. The nanotube arrays were finally transferred onto a flexible printed circuit board, as shown in Fig. 1c. A FESEM image of one of the fabricated sensors is shown in Fig. 1c.

The current–voltage (I – V) characteristics of the ZnO nanotube pressure sensors under different applied pressures were investigated in ambient atmosphere at room temperature. The measurement set-up is shown schematically in Fig. 2a. A VCM with a resolution of 1 mN was

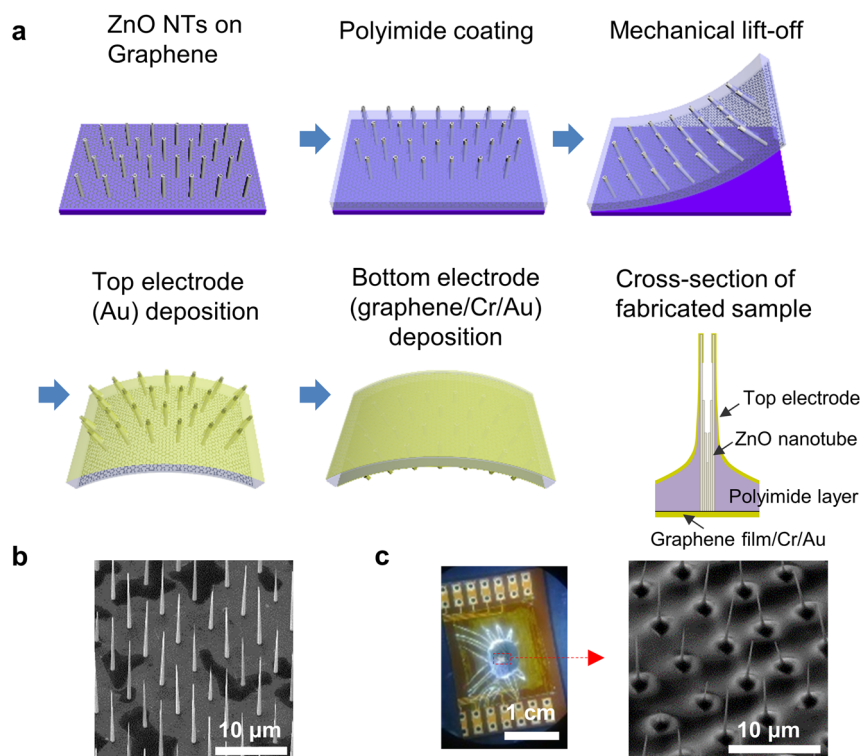


Fig. 1 Fabrication of ZnO nanotube-based pressure sensors. **a** Schematic representation of the stepwise fabrication of the pressure sensors using ZnO nanotube arrays heteroepitaxially grown on graphene layers. The last panel shows a schematic cross-section of the fabricated ZnO nanotube pressure sensors. **b** FESEM image of ZnO nanotube arrays on the graphene substrate. **c** Fabricated flexible ZnO nanotube pressure sensors on the FPCB and corresponding FESEM image.

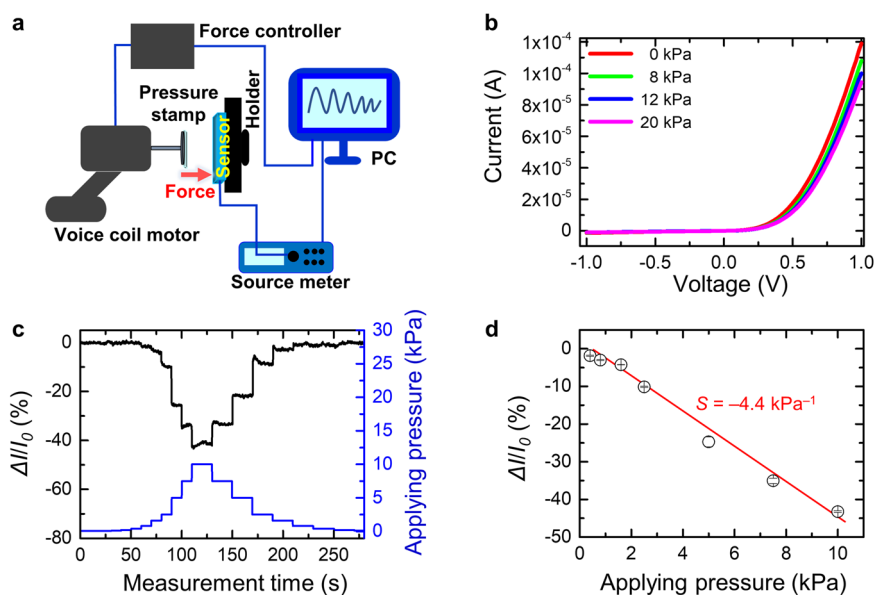


Fig. 2 Current responses of ZnO nanotube pressure sensors. **a** Schematic diagram of the measurement system used to characterize the performance of the ZnO nanotube pressure sensors. The pressure was applied by a VCM. **b** Typical I - V characteristics of the sensors under different applied pressures. **c** Real-time current response of ZnO nanotube pressure sensors under a fixed bias of 0.4 V and with different applied pressures. **d** Current varying ratio ($\frac{\Delta I}{I_0} = \frac{I-I_0}{I_0}$) of ZnO nanotube pressure sensors under different applied pressures. The linear fit indicates a sensitivity of -4.4 kPa^{-1} .

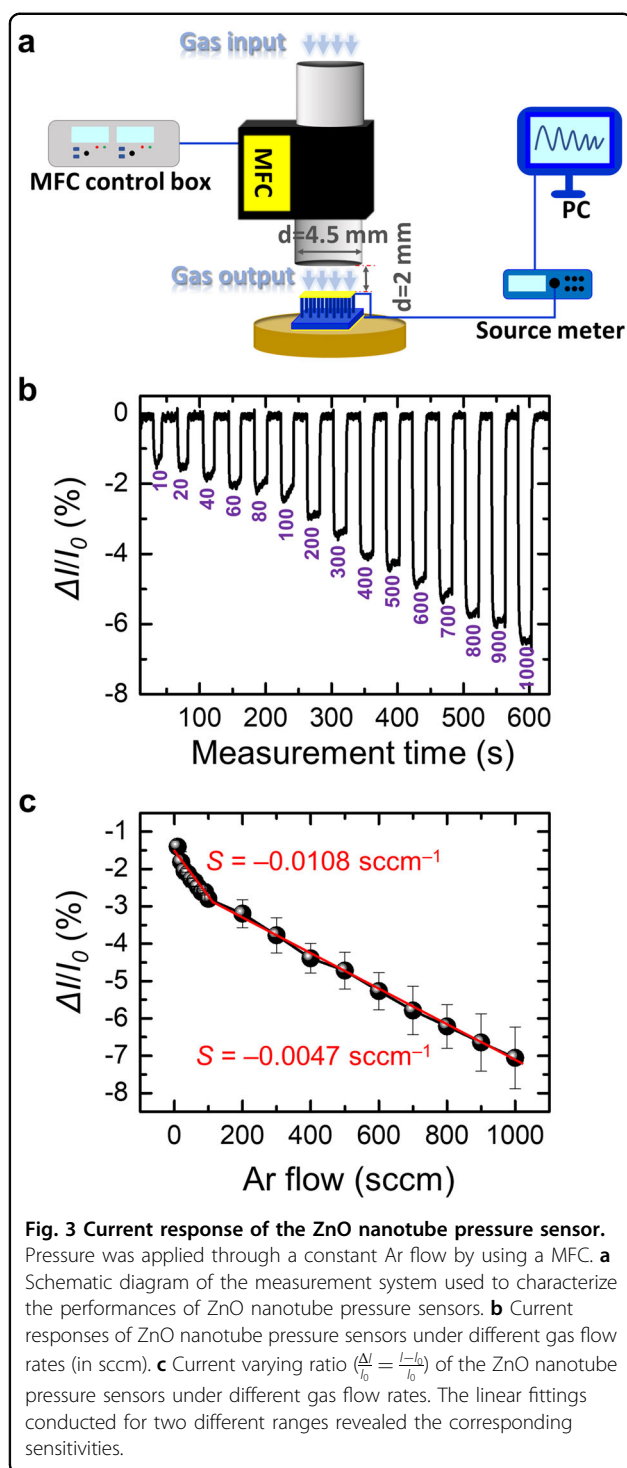
used to apply pressure on the ZnO nanotube sensors, which were fixed to a sample holder on an optical table. The direction of the applied pressure was perpendicular to the surface of the pressure sensor sample. A sapphire substrate was attached as a pressure stamp to electrically insulate the nanotube sensors and the VCM. To distribute the pressure uniformly on the ZnO arrays over an area of 1 mm^2 , a $20\text{-}\mu\text{m}$ -thick PMMA layer was additionally coated on the nanotubes. Figure 2b shows the I – V curves of the ZnO nanotube sensors when voltages of -1 to 1 V were applied under different pressures (between 2 and 10 kPa). The rectifying behavior clearly described by the I – V curves suggests that Schottky and ohmic contacts were well formed on the top (ZnO/Au) and bottom (ZnO/graphene/Cr/Au) sides of the nanotubes, respectively. Under increasing applied pressure, we observed a systematic decrease in current. This can be attributed to a decrease in conductance, which should have been induced by a piezo-induced electric field that formed across the width of the ZnO nanotube when it was bent^{7,25}. This piezo-induced electric field likely trapped charge carriers, creating charge depletion zones on the outer and inner bending surfaces of the nanotubes⁷. A schematic representation describing the pressure-induced charge separation and depletion zone formation is shown in Fig. S2. The piezoelectric potential was compensated by an observed drift in current, which constituted a pressure response²⁶. For estimation of the sensitivity, the applied pressure was increased step by step and then released in a reverse progression. The current variation observed with a constant bias voltage of 0.4 V is shown in Fig. 2c. In response to changes in applied pressure (p), the amount of current moving through the nanotube sensors also showed a systematic variation with ten different steps. The current variation ratio was defined as $\Delta I/I_0 = (I - I_0)/I_0$, where I and I_0 are the currents in the presence and absence of pressure, respectively (plotted as functions of the applied pressure in Fig. 2d). A linear relationship was observed between the current variation ratio and the device sensitivity: $S = \Delta(\Delta I/I_0)/\Delta p = -4.4\text{ kPa}^{-1}$. This sensitivity is comparable to those of other semiconductor nanostructure-based piezoelectric pressure sensors^{27,28}. Due to the presence of the additional PMMA coating (Fig. S3), the device can be assumed to have a sensitivity ~ 2.5 times higher than that measured.

The stabilities and response times of the pressure sensors were also studied. (Figs. S4 and S5). First, a force of 500 mN was applied uniformly over an area of $1 \times 1\text{ mm}^2$ for 12 s as a square wave signal with a duty cycle of 30 h . The current variation ratio showed identical values after 1 h and $>18,000$ repetitions over 30 h (Fig. S4). To determine the response time of the pressure sensors, we periodically compressed them at frequencies of 0.5 , 1 , 5 , and 10 Hz and applied a constant pressure of 2 kPa at a

fixed bias of 0.8 V (Fig. S5a–d). A fast response time ($<100\text{ ms}$) was observed in each case. These results revealed that the proposed nanotube sensors have high durability and reliability, as well as a very fast response time when applied in wearable healthcare devices (e.g., heartbeat²⁹ and breath³⁰ monitors).

To further investigate the sensitivity of the ZnO pressure sensors in the presence of low gas flows, they were subjected to a uniform pressure by using a MFC. The measurement system is shown schematically in Fig. 3a. Notably, at that time, the additional PMMA layer was not coated on the sensors, and accurate sensitivities were realized. Figure 3b shows the real-time current variation ratio measured as the Ar gas flow rate was increased from 10 to 1000 sccm . A significant change in the current variation ratio occurred along with increasing gas flow rate: Fig. 3c shows the current variation ratio as a function of the applied flow rate. A sensitivity of -0.0108 sccm^{-1} was observed when the gas flow rate was $<100\text{ sccm}$, but this value decreased to -0.0047 sccm^{-1} as the gas flow rate was increased. The lower sensitivity measured at higher flow rates was due to an increase in the elastic resistance during the bending of the ZnO nanotubes: in general, a higher pressure is needed to bend ZnO nanotubes that have already been bent once^{8,31–33}. Compared to the unidirectional pressure exerted by a VCM, the pressure direction generated by a gas flow is slightly different. In fact, because of turbulence existing over the surface of pressure sensors, gas molecules apply pressure not only on the top surface of the nanotubes but also on their sidewalls. This likely explains the high current variation ratio observed with ultralow flow rates. Additionally, when the gas flow direction was tilted, most of the gas molecules applied pressure directly on the sidewall of the ZnO nanotubes, leading to an increase in the current variations (Fig. S6).

To investigate the dependence of the sensors on nanotube dimensions, we fabricated ZnO nanotube pressure sensors with different wall thicknesses. Figure 4a shows FESEM images of ZnO nanotube pressure sensors with wall thicknesses of 30 , 210 , and 300 nm and a fixed height of $18\text{ }\mu\text{m}$. The wall thickness of the as-grown ZnO nanotubes was 30 nm . To increase the lateral growth of the nanotubes, we grew them in the reactor of the MOCVD chamber with a relatively low temperature and high pressure. During this process, the outer shape of the nanotubes changed, and the shape of their cross-sections changed from a smooth circle-like polygon to a hexagon. In addition, the open hole of the inner core of the nanotube end tip changed into a closed solid (Fig. 4a). Figure 4b shows the real-time current variation ratio as a function of flow rate for nanotube sensors with different wall thicknesses. The current ratios dramatically decreased with increasing nanotube



wall thickness. The sensitivities of nanotubes with thicknesses of 30, 210, and 300 nm at gas flow rates <200 sccm were -0.0186 , -0.0097 , and $-0.0055 \text{ sccm}^{-1}$, respectively, while at gas flow rates >200 sccm, they were -0.0059 , -0.0028 , and $-0.0019 \text{ sccm}^{-1}$, respectively.

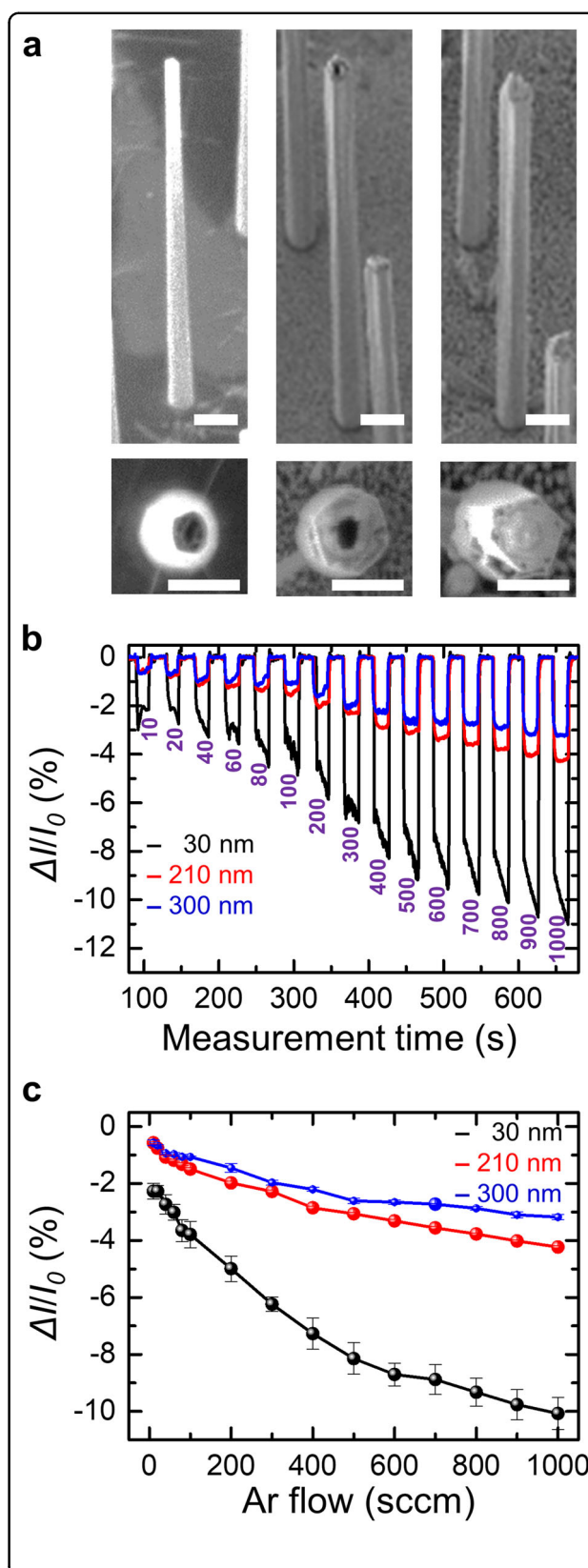


Fig. 4 Pressure responses of nanotube sensors with different wall thicknesses. **a** FESEM images of ZnO nanotubes with wall thicknesses of 30, 210, and 300 nm and the same length (18 μm). The top and bottom panels show tilted and cross-sectional views, respectively. The scale bars in the top and bottom panels are 1 μm and 500 nm, respectively. **b** Current variation ratio as a function of flow rate with different wall thicknesses. The unit of numbers (in purple color) is sccm. **c** Comparison of the corresponding current response of the ZnO nanotube pressure sensor as a function of the applied flow rate.

(Fig. 4c). We infer that the higher sensitivity of the thinnest nanotubes was related to their elastic modulus. Furthermore, it can be inferred that nanotubes with smaller thickness possess a larger dielectric than thicker tubes. Hence, higher sensitivity and better device performance are obtained for sensors with thinner nanotubes.

Pressure responses of nanotubes with different lengths were also investigated. Figure 5a shows FESEM images of fabricated ZnO nanotube sensors, which reached lengths of 7, 12, and 18 μm after 1, 2, and 3 h of vertical growth, respectively. Due to the thickness of the PI layer (5 μm), the exposed lengths of the ZnO nanotubes in the FESEM images were 2, 7, and 12 μm . The wall thickness of the ZnO nanotubes finally reached 300 nm after 4 h of lateral growth followed by vertical growth. Figure 5b shows the real-time current variation ratio as a function of flow rate for nanotube sensors with different wall thicknesses. The longest nanotubes showed higher sensitivities, which was related to a smaller elastic modulus. The sensitivities of ZnO nanotubes with lengths of 7, 12, and 18 μm were -0.0055 , -0.0047 , and -0.0003 sccm $^{-1}$, respectively, under low gas flow rates (<200 sccm) but were -0.0019 , -0.0014 , and -3×10^{-5} sccm $^{-1}$, respectively, under high gas flow rates (>200 sccm) (Fig. 5c). Overall, these characteristics indicated that nanotubes with thinner walls and greater lengths had higher pressure sensitivities. This demonstrates how nanotube structures can be advantageous for ultrahigh sensitivity applications: they support the creation of structures with very high aspect ratios and ultrathin walls.

In addition to high sensitivity and durability, the proposed nanotube sensors showed reliable I - V characteristics and uniform response under mechanically bent conditions (Fig. S7d, e). Although the effective dimension of the sensor was 1 mm 2 , the sensor could resolve the force/pressure from any part of the sensor (Fig. S8). Additionally, the sensors respond to a simple touch, as shown in Fig. S9. These properties are promising for their application in wearable healthcare monitoring devices. To demonstrate the validity of this hypothesis, we used nanotube sensors for the detection of human breath and pulses. First, one of the proposed sensors was attached on the philtrum of a volunteer to detect their breath (Fig. 6a). Significant changes were observed in the current variation

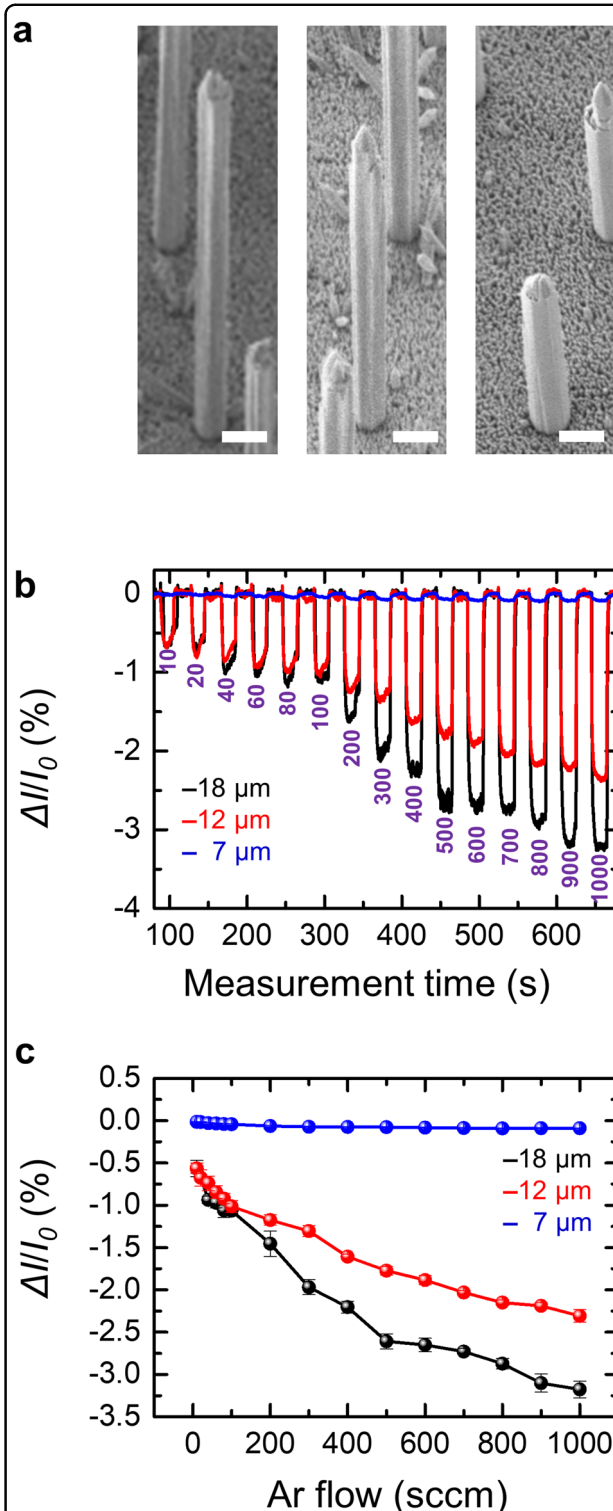


Fig. 5 Pressure responses of nanotube sensors with different lengths. **a** FESEM images of ZnO nanotubes with lengths of 18, 12, and 7 μm . The length of each scale bar equals 1 μm . **b** Current variation ratio for different lengths and as a function of flow. The numbers at the bottom of the curves in purple denote flow in sccm. **c** Current responses of the ZnO nanotube pressure sensors as a function of different flow rates.

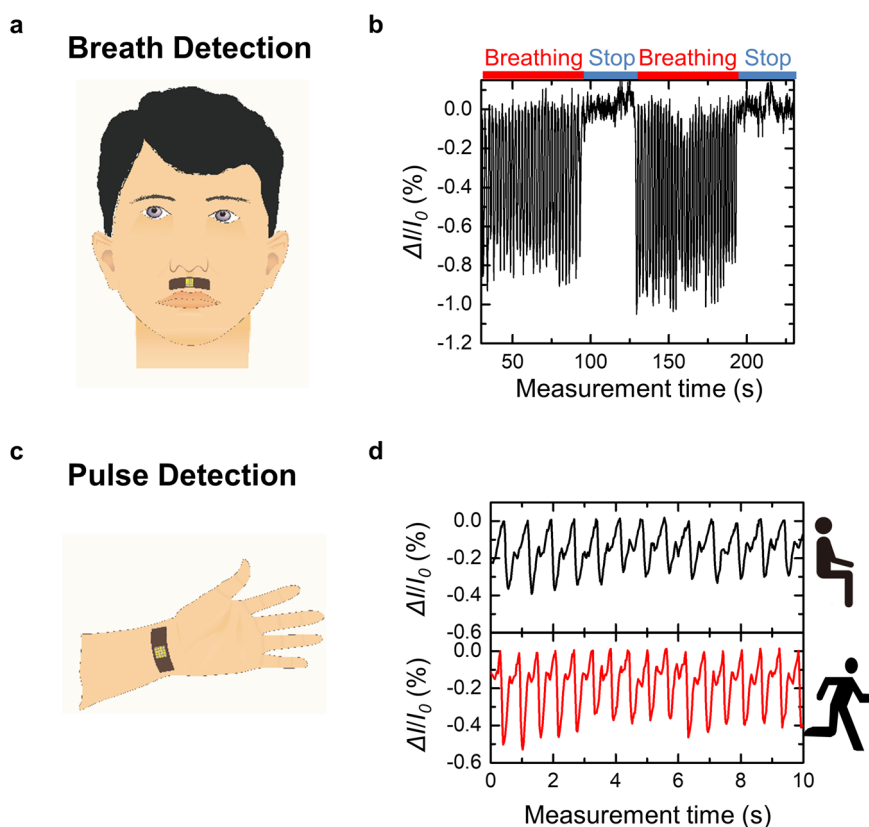


Fig. 6 Testing of biomedical applications based on flexible ZnO nanotube pressure sensors. **a** Schematic representation of the fabricated pressure sensor directly attached to the philtrum of a volunteer for breath detection. **b** Real-time current response of the ZnO pressure sensor during breath monitoring. **c** Schematic representation of the fabricated pressure sensor directly attached to the wrist of a volunteer for pulse detection. **d** Real-time current response of the ZnO pressure sensor during pulse monitoring before and after running.

ratio between normal breathing and hold conditions (Fig. 6b). Respiration rates of 15–25 per min, corresponding to the normal breath rates of an adult person at rest, were determined during normal breathing. These results indicate that our sensors can be used to detect a simple pause in normal breathing, as in the case of sleep apnea. The monitoring of heartbeat rates was also tested on a volunteer both at rest and after a short workout (running) by placing one of our flexible sensor devices on his wrist (Fig. 6c). The corresponding pulse waveforms are shown in Fig. 6d. We measured 13 pulses per 10 s at rest and 16 pulses per 10 s after running. The amount of current variation ratio (i.e., the depth of pulse) increased by up to 25% after running due to the faster heartbeat. Overall, these results prove the possibility of using our ZnO pressure sensors to monitor physiological parameters in daily life.

Conclusions

Piezoelectric pressure sensors were fabricated by using vertically aligned and position- and dimension-controlled ZnO nanotube arrays grown on graphene layers. Due to

the ultrathin walls and high aspect ratios of the ZnO nanotubes, these sensors exhibited high sensitivity. In addition, they showed a fast response time, a stable response with enormous durability, and mechanical flexibility. Considering these promising properties, we tested the possibility of applying such sensors to wearable health monitoring devices. Human breath and pulse rates were successfully detected with high signal-to-noise ratios. Overall, the results demonstrated the high potential of the proposed sensors for application in wearable electronic devices aimed at diagnosis of early-stage pulmonary and cardiovascular diseases.

Acknowledgements

This work was financially supported by the Samsung Research Funding Center of Samsung Electronics (SRFC-TA1803-02(0417-20180116)).

Author details

¹Department of Physics and Astronomy and Institute of Applied Physics, Seoul National University, Seoul 08826, South Korea. ²Department of Electrical and Computer Engineering, University of California San Diego, La Jolla, CA 92093, USA. ³Institute for Photonics and Quantum Sciences, SUPA, Heriot-Watt University, Edinburgh EH14 4AS, UK. ⁴Department of Materials, Imperial College London, London SW7 2BU, UK. ⁵School of Materials Science and Engineering,

Sungkyunkwan University, Suwon 16419, South Korea. ⁶Research Institute of Advanced Materials, Seoul National University, Seoul 08826, South Korea

Author contributions

J. B. P.: Conceptualization, methodology, investigation, data curation, formal analysis. M. S. S.: Methodology, formal analysis, investigation, writing—review & editing. R. G.: Methodology, formal analysis, investigation, writing—review & editing. R. K. S.: Methodology. Y. H.: Methodology, investigation. Y. T.: Investigation. H. O.: Investigation. H. B.: Investigation, writing—review & editing. Y. L.: Investigation, writing—review & editing. B. K.: Investigation, validation. S.-W. K.: Investigation, validation. G.-C. Y.: Writing—original draft, formal analysis, conceptualization, project administration, funding acquisition.

Conflict of interest

The authors declare no competing interests.

Publisher's note

Springer Nature remains neutral with regard to jurisdictional claims in published maps and institutional affiliations.

Supplementary information The online version contains supplementary material available at <https://doi.org/10.1038/s41427-021-00324-w>.

Received: 15 February 2021 Revised: 28 June 2021 Accepted: 7 July 2021.
Published online: 30 July 2021

References

- Wang, Z. L. Progress in piezotronics and piezo-phototronics. *Adv. Mater.* **24**, 4632–4646 (2012).
- Bao, R. et al. Flexible and controllable piezo-phototronic pressure mapping sensor matrix by ZnO NW/p-polymer LED array. *Adv. Funct. Mater.* **25**, 2884–2891 (2015).
- Choi, M. Y. et al. Mechanically powered transparent flexible charge-generating nanodevices with piezoelectric ZnO nanorods. *Adv. Mater.* **21**, 2185 (2009).
- Lee, K. Y., Gupta, M. K. & Kim, S. W. Transparent flexible stretchable piezoelectric and triboelectric nanogenerators for powering portable electronics. *Nano Energy* **14**, 139–160 (2015).
- Oh, H. & Dayeh, S. A. Physics-based device models and progress review for active piezoelectric semiconductor devices. *Sensors* **20**, 3872 (2020).
- Ha, M. et al. Bioinspired interlocked and hierarchical design of ZnO nanowire arrays for static and dynamic pressure-sensitive electronic skins. *Adv. Funct. Mater.* **25**, 2841–2849 (2015).
- Wang, Z. L. & Song, J. Piezoelectric nanogenerators based on zinc oxide nanowire arrays. *Science* **312**, 242–246 (2006).
- Hu, W. G., Zhang, C. & Wang, Z. L. Recent progress in piezotronics and triboelectronics. *Nanotechnology* **30**, 042001 (2019).
- Ghosh, R. et al. Fabrication of piezoresistive Si nanorod-based pressure sensor arrays: a promising candidate for portable breath monitoring devices. *Nano Energy* **80**, 105537 (2021).
- Peng, M. et al. High-resolution dynamic pressure sensor array based on piezo-phototronic effect tuned photoluminescence imaging. *ACS Nano* **9**, 3143–3150 (2015).
- Song, M. et al. Flexible Li-doped ZnO piezotronic transistor array for in-plane strain mapping. *Nano Energy* **55**, 341–347 (2019).
- Liu, C. et al. Interface engineering on p-CuI/n-ZnO heterojunction for enhancing piezoelectric and piezo-phototronic performance. *Nano Energy* **26**, 417–424 (2016).
- Tchoe, Y. et al. Individually addressable, high-density vertical nanotube Schottky diode crossbar array. *Nano Energy* **76**, 104955 (2020).
- Tchoe, Y. et al. Free-standing and ultrathin inorganic light-emitting diode array. *NPG Asia Mater.* **11**, 37 (2019).
- Hu, C. H., Liu, C. H., Chen, L. Z., Peng, Y. C. & Fan, S. S. Resistance-pressure sensitivity and a mechanism study of multiwall carbon nanotube networks/poly(dimethylsiloxane) composites. *Appl. Phys. Lett.* **93**, 033108 (2008).
- Gong, S. et al. A wearable and highly sensitive pressure sensor with ultrathin gold nanowires. *Nat. Commun.* **5**, 3132 (2014).
- Tee, B. C. K., Wang, C., Allen, R. & Bao, Z. An electrically and mechanically self-healing composite with pressure- and flexion-sensitive properties for electronic skin applications. *Nat. Nanotechnol.* **7**, 825 (2012).
- Zhao, Z. et al. Piezotronic effect in polarity-controlled GaN nanowires. *ACS Nano* **9**, 8578–8583 (2015).
- Hong, Y. J. et al. Controlled epitaxial growth modes of ZnO nanostructures using different substrate crystal planes. *J. Mater. Chem.* **19**, 941–947 (2009).
- Park, J. B. et al. Scalable ZnO nanotube arrays grown on CVD-graphene films. *APL Mater.* **4**, 106104 (2016).
- Kim, Y. J. et al. Position- and morphology-controlled ZnO nanostructures grown on graphene layers. *Adv. Mater.* **24**, 5565–5569 (2012).
- Perea, D. E. et al. Three-dimensional nanoscale composition mapping of semiconductor nanowires. *Nano Lett.* **6**, 181–185 (2006).
- Noborikasa, J., Motohisa, J. & Fukui, T. Catalyst-free growth of GaAs nanowires by selective-area metalorganic vapor-phase epitaxy. *Appl. Phys. Lett.* **86**, 213102 (2005).
- Wang, Y. G., Yuen, C., Lau, S. P., Yu, S. F. & Tay, B. K. Ultraviolet lasing of ZnO whiskers prepared by catalyst-free thermal evaporation. *Chem. Phys. Lett.* **377**, 329–332 (2003).
- Zhang, Z. Q., Geng, D. L. & Wang, X. D. Calculation of the piezoelectric and flexoelectric effects in nanowires using a decoupled finite element analysis method. *J. Appl. Phys.* **119**, 154104 (2016).
- Wang, X. et al. Piezoelectric field effect transistor and nanoforce sensor based on a single ZnO nanowire. *Nano Lett.* **6**, 2768–2772 (2006).
- Chen, W. F. & Yan, X. Progress in achieving high-performance piezoresistive and capacitive flexible pressure sensors: a review. *J. Mater. Sci. Technol.* **43**, 175–188 (2020).
- Li, L. et al. Flexible pressure sensors for biomedical applications: from ex vivo to in vivo. *Adv. Mater. Interfaces* **7**, 2000743 (2020).
- Shin, K. Y., Lee, J. S. & Jang, J. Highly sensitive, wearable and wireless pressure sensor using free-standing ZnO nanoneedle/PVDF hybrid thin film for heart rate monitoring. *Nano Energy* **22**, 95–104 (2016).
- Xu, X. X. et al. Novel and dual-mode strain-detecting performance based on a layered NiO/ZnO p-n junction for flexible electronics. *J. Mater. Chem. C* **8**, 1466–1474 (2020).
- Wu, W. Z., Wen, X. N. & Wang, Z. L. Taxel-addressable matrix of vertical-nanowire piezotronic transistors for active and adaptive tactile imaging. *Science* **340**, 952–957 (2013).
- Soomro, M. Y. et al. Nanoscale elastic modulus of single horizontal ZnO nanorod using nanoindentation experiment. *Nanoscale Res. Lett.* **7**, 146 (2012).
- Manoharan, M. P., Desai, A. V., Neely, G. & Haque, M. A. Synthesis and elastic characterization of zinc oxide nanowires. *J. Nanomater.* **2008**, 849745 (2008).